

Gamma-Ray Computed Tomography in Soil Science: Some Applications

Luiz Fernando Pires¹, Fábio Augusto Meira Cássaro¹,
Osny Oliveira Santos Bacchi² and Klaus Reichardt²

¹*State University of Ponta Grossa, Department of Physics*

²*Center for Nuclear Energy in Agriculture, Laboratory of Soil Physics
Brazil*

1. Introduction

The first computed tomography (CT) apparatus was developed by Godfrey Hounsfield, at the beginning of the seventies of the last century (Hounsfield, 1973). For its development Hounsfield and Allan M. Cormack (Cormack, 1963), who developed the mathematical basis of image reconstruction, were rewarded by the Nobel Prize in medicine in 1979. Cormack's developments were basically focused in the reconstruction of bodies with geometries with no medical interest, like for instance, the human head.

After these first developments, some CT scanners were developed and gradually introduced into other areas of knowledge like engineering, agronomy, biology, physics, chemistry, etc. Most of the modern scanners make use of gamma and X-ray sources. However some instruments make use of neutron and positron ray sources.

Recent developments describe the use of synchrotron X-ray beams to investigate fluid transport at the pore scale (Coles et al., 1998). Some other applications of CT involve: investigation on morphological changes in small animals (Stenstrom et al., 1998); determination of soil macroporosity by chemical mapping (Brandsma et al., 1999); and dental analysis of the anatomy and some restorative materials through X-ray microtomography (Braz et al., 2001). More recently, Vontobel et al. (2006) and Winkler et al. (2006) presented the use of neutron tomography to investigate the morphology or structure of rocks and metal melts. CT allowed demonstrating the behaviour of metal melts with different densities. Voronov et al. (2010) used the micro CT (with micrometric resolution) to analyze the distribution of flow-induced stresses in highly porous media of interest for bioengineering. Flow-induced stresses have been found to stimulate the growth of cells.

Reports describing the use of the CT in soil science were published few years later of the invention of the first tomography scanner system by Hounsfield. Petrovic et al. (1982) followed by Hainsworth and Aylmore (1983) and Crestana et al. (1985) successfully reported the use of CT scanners for soil bulk density studies, soil water content and water movement measurements.

CT is a non destructive and non invasive investigation technique used to assess some attributes in the interior of an object of interest. It is essentially based on the principle of the attenuation of an electromagnetic radiation beam by the object. CT technique has been well

accepted in agricultural research, due to its non invasive and non destructive characteristics, which allow repeated measurements on the same sample that does not need any pre treatment. Another important fact is that modern scanners allow investigating a sample with increasingly better resolutions. It is also important to mention that conventional image analysis techniques commonly used in soil physics (Horgan, 1998; Li et al., 2004; Pires et al., 2008) inevitably destroy the inner structure of the soil or do not allow a second measurement at the same position.

In soil science, Phogat et al. (1991) showed the potential of the use of dual-gamma energy CT for non destructive studies of the structural status and stability of soils. Rasiah and Aylmore (1998) used CT to analyze the influence of wetting and differences in structural stability on the spatial continuity of soil parameters. Perret et al. (1999) using the CT determined the geometry and topology of macropore networks. Gantzer and Anderson (2002) measured the macroporosity of soils affected by different tillage managements. Langmaack et al. (2002) and Jégou et al. (2002) studied soil rehabilitation after earthworm activities. Appoloni et al. (2002) applied X-ray microtomography to investigate thin layers of soil clod particulate systems and porous microstructures. Baveye et al. (2002) showed the importance of soil sampling volume in the determination of macroscopic parameters, like volumetric water content, volumetric air content, gravimetric water content, and bulk density. Wildenschild et al. (2002) have compared three different X-ray CTs to characterize hydrological soil properties. Elliot and Heck (2007) proposed the CT as a complementary methodology of the optical method for void space determination. In Taina et al. (2008) an interesting and vast literature review is presented for the application of X-ray CT to soil science.

In Brazil, soil science studies were firstly carried out using CT medical scanners. However, their high costs and difficulties involved in their calibrations for soil investigations make them practically unavailable for this kind of studies. This problem was solved by developing cheaper dedicated 1st generation CT scanners, designed for specific use in agronomy research (Cesareo and Giannini, 1980; Cesareo et al., 1994; Crestana et al., 1986; Cruvinel et al., 1990; Naime, 1994; Naime, 2001). Nowadays, some research groups in Brazil have been conducting studies using scanners of 1st and 3rd generation, which use gamma or X-ray radiation sources; most of their studies are in the millimetric or micrometric resolution level.

The use of CT for measurements of soil water retention and movement was introduced in Brazil by Crestana et al. (1985). Afterwards, Vaz et al. (1989), using a gamma-ray tomograph with millimetric resolution evaluated soil bulk density modifications due to conventional management practices. Cruvinel et al. (1990) presented the development of a 1st generation CT scanner which makes use of X-ray (60 kVp, 60 mA) or gamma-ray (^{241}Am , 60 keV, 300 mCi) sources, exclusively for soil physics research in Brazil. Biassusi et al. (1999) presented an investigation of soil bulk density changes in a swelling soil submitted to several hydration levels. Lopes et al. (1999) showed that the neutron tomography is able to detect small differences in soil moisture and that the methodology using neutrons provides more representative results of soil moisture variations in comparison to CT using gamma-rays. Fante Júnior et al. (2002) compared the methods of the paraffin sealed clod and CT for soil bulk density evaluations and found a good correlation between these two methods. Nonetheless, CT has the additional advantage of being a non-destructive measurement method that allows the measurement of soil density with a spatial resolution of millimeters. Pedrotti et al. (2003) described aspects of the choice of sample size for measurements of soil

density by CT. Balogun and Cruvinel (2003) employed Compton scattering CT to study the soil density distribution inside samples with different degrees of compaction. Pires et al. (2004) applied CT in studies of soil structure disturbance produced by traditional sampling methods. Pires et al. (2007) used the CT technique to evaluate the radius of influence of tensiometer and soil solution extractors in field measurements. Modolo et al. (2008) used a 3rd generation microtomograph scanner to analyze changes produced by soybean seeding procedures in a non-tillage management field. In Pires et al. (2011a), the use of CT is presented to investigate the modifications that might occur in soil samples submitted to several wetting and drying cycles. A better picture of the use of CT technique applied to soil science investigation, in the past 25 years, in Brazil can be found in Pires et al. (2010).

This chapter presents some possible uses of single energy gamma-ray computed tomography (GCT) applied to soil science studies, such as: 1) soil bulk density (ρ_s) and soil porosity (ϕ) detailed determinations, 2) soil crust characterization, and 3) soil structure changes.

2. Theoretical background

2.1 Interaction of radiation with matter

Alpha and beta particles and gamma and X-radiation interact with matter in completely different ways. Due to their charges and masses alpha and beta particles interact with matter producing excitations and ionizations, what makes them lose rapidly their energy during the interaction. In the case of X and gamma-radiation, which is composed by photons, the interaction with matter is basically via: the photoelectric effect, Compton scattering, and pair production (for photons with energies higher than 1.02 MeV). These interactions make the attenuation of the radiation by matter to follow an exponential behaviour (Kaplan, 1963). The energy of the gamma-photons of interest in soil science falls in the range between 50 and 700 keV. The characteristic of an absorbing material to scatter or absorb a photon is called the attenuation coefficient. The linear attenuation coefficient (κ , cm^{-1}) represents the probability of absorption of a photon beam per unit path length (Chase and Rabinowitz, 1968). It is dependent of the density of the absorbing material (ρ , g cm^{-3}). For example, even being composed by the same material ice, water, and steam have different linear attenuation coefficients (Ferraz and Mansell, 1979). Nevertheless the mass attenuation coefficient μ (κ/ρ , $\text{cm}^2 \text{g}^{-1}$) of these materials are the same and are frequently tabulated as the probability of an individual element to attenuate a determined type of gamma or X-ray radiation (Jenkins et al., 1981).

For a given composit material, κ corresponds to the sum of all its chemical components (Kaplan, 1963):

$$\kappa = \sum \kappa_i w_i \quad (1)$$

where w_i represents the weight fraction of component i in the absorbing material.

The change in intensity “ ΔI ” of a gamma or X-ray beam interacting with an absorber of thickness, Δx (cm) is given by:

$$\Delta I = -\kappa I \Delta x \quad (2)$$

When integrated this relation provides the Beer-Lambert equation, which relates I_0 and I , the intensities of the beam before and after passing through the absorber, respectively (Colgate, 1952; Wang et al., 1975):

$$I = I_0 \exp(-\kappa x) \quad (3)$$

For heterogeneous systems x is considered as the sum of the length x_i of the path corresponding to each component i . For the case of soils, this summation is made over soil solid component (soil particles), soil liquid component (soil solution), and soil gaseous component (soil air). As the attenuation of the air is negligible in comparison with the other components equation (3) can be rewritten as follows (Ferraz and Mansell, 1979):

$$I = I_0 \exp(-(\kappa_w x_w + \kappa_s x_s)) = I_0 \exp(-(\mu_w \rho_w \theta + \mu_s \rho_s) x) \quad (4)$$

where the subscripts s and w stand for soil and water, respectively, and θ is the volumetric soil water content ($\text{cm}^3 \text{cm}^{-3}$). The density of water ρ_w (g cm^{-3}) is generally considered as unity. From equation (4) it follows that (Cesareo et al., 1994):

$$\kappa = \mu_s \rho_s + \mu_w \theta \rho_w \quad (5)$$

and it becomes clear that measurements of κ provide information about soil bulk density and soil water content. Therefore, it is possible to evaluate these soil properties using X or gamma-ray attenuation techniques (Elzefrawy et al., 1976; Ferraz, 1974).

2.2 Basic principles of computed tomography

When n regions with different thicknesses and different linear attenuation coefficients are placed along a radiation beam, the Beer-Lambert law (Equation 3) can be written as (Herman, 1980):

$$I = I_0 \cdot \exp\left(-\sum_{j=1}^n \kappa_j x_j\right) \quad (6)$$

Having a set of simple transmission measurements, obtained in different orientations across a plane of an object makes it possible to map the attenuation coefficients of the material in this selected plane.

The method used for image reconstruction uses mathematical manipulation to generate a unit called TU (tomographic unit) that is assigned to each position of the plane (Vaz et al., 1989). Different colours or gray intensity values are assigned to these units, what permits to visualize or investigate the image or tomography of the plane. For instance, the tone of one point of the image can vary from white (no attenuation of the beam) to black (maximum attenuation of the beam), passing through different gray tonalities depending on intermediate degrees of interaction of the object with the beam (Brooks et al., 1981).

When a tomographic image is obtained for a heterogeneous material, the beam will cross different directions in a chosen plane of the sample and travel through regions of distinct physical properties with different thicknesses l . For the reconstruction of the image with a heterogeneous distribution of densities it is necessary to use a coordinate system (x, y) on the chosen plane to locate the measured points. In the tomographic analysis the intensity of the emerging beam is proportional to the integral of all $\mu(x, y)$ of a given path L , which is represented by the straight line for a particular source-detector pair arrangement (Kak and Slaney, 1988):

$$\ln\left(\frac{I_0}{I}\right) = \int_{r,\varphi} \kappa(x, y) dl \quad (7)$$

where dl denotes the integration along the beam path, the subscript r represents the measurements made in different parallel paths separated by a constant distance Δr and φ is the rotation angle of the sample, made in regular steps $\Delta\varphi$ around the line formed by source and detector.

Mathematically it is possible to define a function $f(x, y)$, called density function M , which represents the distribution of a given physical property M along a cross section of the sample. The main objective of CT is to reproduce as precisely as possible the function $f(x, y)$, which represents the attenuation coefficient κ of the slice of the material, that in turn is related to M . The line integral of this function in relation to (r, φ) is called ray sum or projection ray $P(r, \varphi)$, given by (Herman, 1980):

$$P(r, \varphi) = \int_{r, \varphi} f(x, y) dl \quad (8)$$

When $f(x, y)$ represents $\kappa(x, y)$ it is possible to obtain a set of ray sums using equations (7) and (8), for a defined angle φ , called projection. Acquiring a large number of projections for different values of φ it is possible to construct the function $f(x, y)$, which will provide a 2D image (composed of squares called pixels with a gray level that is related to its density) of the slice (Martz et al., 1990).

2.3 Computed tomography calibration

The evaluation of soil physical properties like bulk density and water content using CT depends on the calibration of the system, that basically consists in finding a relation between TU and κ for some 'homogeneous' materials.

The tomographic unit, which is related to κ of the soil in each crossing position, takes the air as the medium with the minimum possible κ value. In the case of heterogeneous materials like soils, TU is a result of the contributions from solid mineral and organic components, water, and air crossed by the radiation beam, which makes κ different for each path through the sample. Attenuation of the beam by the air is insignificant as compared to soil particles and water, and it can therefore be neglected. For a dry soil sample the relation between TU and κ is given by:

$$TU = \alpha\kappa = \alpha (\mu_s \rho_s) \quad (9)$$

For example, if the value of TU obtained by CT scanning is known for a given portion of a soil, the value μ_s is determined by gamma-ray attenuation measurements and the value of α is also known, it is possible to determine ρ_s using equation (9).

The choice of materials for the calibration determines the goodness of fitting between TU and κ . In general, homogeneous materials produce better calibration fittings than heterogeneous materials like soils (Figure 1).

During the CT calibration κ of each material is determined using the Beer-Lambert law, and in general represents an average of several measurements taken in different positions of this material. Values of TU are extracted from the tomographic images (Vaz et al., 1989; Crestana et al., 1992; Pires et al., 2011b).

3. Gamma-ray CT scanner

The results presented in this work were obtained with a first generation CT scanner with a fixed source-detector arrangement and translation/rotational movements of the samples (Figure 2).

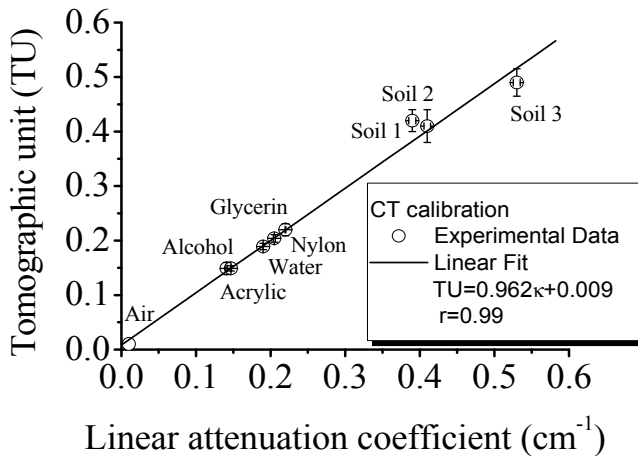


Fig. 1. Computed tomography (CT) calibration curve for ²⁴¹Am gamma-ray radiation. Error bars represent the standard deviation of the measurements. Soil 1, 2 and 3 are sand, clay loam and clay sieved soils.

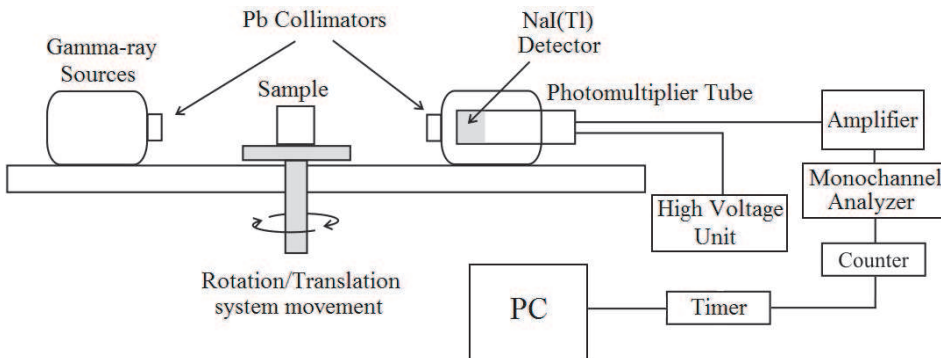


Fig. 2. Schematic diagram of a first generation CT scanner. Adapted from Pires et al. (2011c).

The radioactive sources used in the study were ²⁴¹Am (59.54 keV) and ¹³⁷Cs (661.6 keV), protected by a lead block. A NaI(Tl) scintillation crystal (7.62 × 7.62 cm) coupled to a photomultiplier tube was used to detect the monoenergetic photons passing through cylindrical lead collimators placed either in front of the source as the detector (Figure 3). The gamma detector is also protected by a lead block to minimize background radiation detection. The acquired data were stored in a PC and CT images were obtained using the reconstruction algorithm Microvis (2000).

The angular and linear steps were chosen as: 2.25° and 0.11 to 0.15 cm, respectively.

4. Soil science applications

This section presents some applications of the gamma-ray computed tomography (GCT) in soil science. The analyses were accomplished with the first generation scanner shown at

the last section, which has millimetric resolution. Qualitative and quantitative results were obtained by examining 2D images of soil sample sections. The following applications will be presented to give a general notion of the power of GCT as a tool for soil science studies.

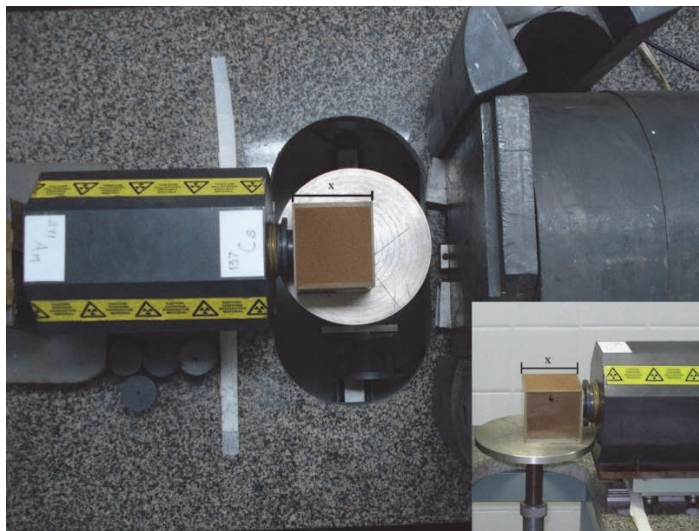


Fig. 3. Picture of the gamma-ray CT scanner located at the Laboratory of Soil Physics (Center for Nuclear Energy in Agriculture, Piracicaba, Brazil). At the left side there is the gamma-ray source, at the center the sample and at the right side the lead block covering the gamma detector and photomultiplier tube. Courtesy of Costa (2011).

4.1 Application of GCT to study soil bulk density and porosity

In this item the use of GCT is presented as a tool to obtain detailed information of soil bulk density and porosity distributions.

The soil bulk density is represented by the ratio of the mass of the solid phase of the soil for its total volume, and is determined using dried samples, i.e. samples of which the liquid phase was eliminated of its total volume using an oven at 105 °C until constant weight.

The soil porosity represents the portion of the total soil volume not occupied by soil solids. Sample features such as structure, texture and organic matter content largely influence soil porosity. Same values of soil porosity can be related to completely different soil structures and pore distributions.

By soil bulk density or porosity characterization it is possible to obtain important information about soil quality. For example, compacted soils have a much lower porosity. Soil compaction causes modifications on soil porosity and structure that are related to soil water and gas movement inside them. Soil porosity modification has as consequence the decrease of water infiltration rate, which in turn can increase the water runoff volume on soil surface which is related, for example, to furrow irrigation erosion.

Tomographic images of two soil clod samples are shown in figure 4, collected from the soil surface (0-10 cm).

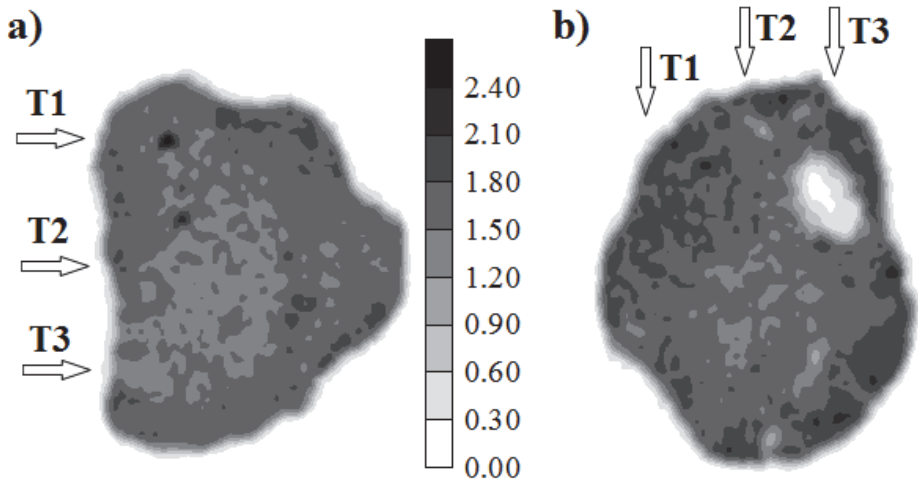


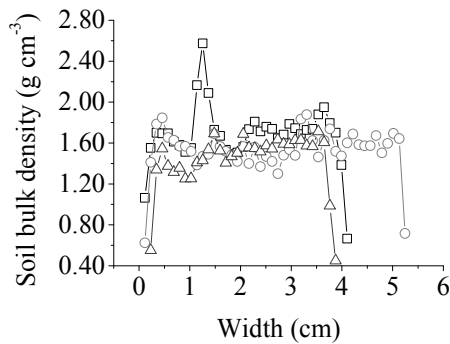
Fig. 4. (a,b) Tomographic images of soil clods collected from soil surface. T1, T2, and T3 represent transects used for quantitative soil bulk density (ρ_s) analysis. The gray scale represents the distribution of ρ_s , where white refers to the lowest ρ_s value and black to the highest.

As it can be seen in figure 4 tomographic images permit firstly a qualitative analysis of soil structure. For example, it is possible to observe dense regions (dark gray spots) and great holes (light gray or white spots) (Figures 4a and 4b) inside the soil samples. Denser regions inside the sample are probably related to stones inside the soil while the less dense regions are in general related to macropores (*e.g.* biopores caused by worms or roots).

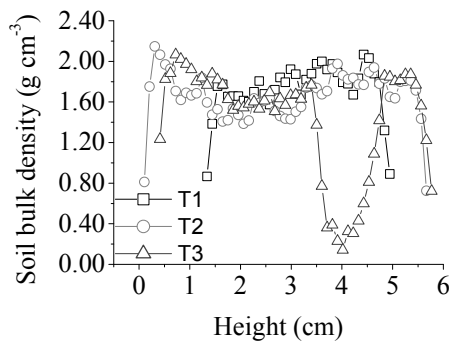
From the images it is possible to obtain a 2D arrangement of tomographic units and consequently the global density distribution inside the investigated sample. Another advantage of the technique is that modifications inside the sample can be followed by redoing the image after any treatment imposed on it, something that is not possible by the traditional techniques such as the paraffin clod method for bulk density determination.

Using tomographic images it is possible to investigate the soil bulk density distribution and variability inside a sample. Figures 5a and 5b present ρ_s values inside samples, at each 0.115 cm (Figure 5a) and at each 0.104 cm (Figure 5b), along the linear transects T1, T2, and T3 presented in figures 4a and 4b.

From these figures some very distinct values of bulk density can be observed inside the sample. Generally these values are related to the presence of stones and holes. Along T1 of figure 5a, a global density of 2.57 g cm^{-3} can be noticed, a value close to the average stone density of 2.65 g cm^{-3} , which represent the very dark point in figure 4a. On the other hand, low bulk density values are related to holes in the sample. An example of this is observed in T3 of the second investigated clod (Figures 4b and 5b). Using information extracted from the images and the transects it is also possible to calculate an approximation of the area occupied by the hole, 1.17 cm^2 , which can be related to the presence of a dead root or a wormhole.



(a)



(b)

Fig. 5. Soil bulk density (ρ_s) values along linear transects (T) inside the soil clods. (a) Analysis along soil width and (b) analysis along soil height.

The average bulk density values resulted from the GCT analysis were 1.57 ± 0.06 and 1.62 ± 0.10 g cm^{-3} for clods A and B, respectively. Comparable values of ρ_s were obtained by the paraffin sealed clod method, average of 1.56 g cm^{-3} for these clods. The GCT technique was also used for determining the porosity (ϕ) of the samples. By the traditional method this determination is made by using soil bulk density and soil particle density (ρ_p) values, using the following expression (Flint and Flint, 2002):

$$\phi = (1 - \rho_s / \rho_p) \cdot 100 \quad (10)$$

One artificially packed soil sample in a cylindrical container of 5.0 cm in diameter was produced to show the potential of the GCT for ϕ analysis (Figure 6). To prepare the sample, 2.0 mm sieved air-dry soil was homogeneously packed in the cylinder. The tomographic image represents a cross section taken at the middle of the sample.

By the analysis of the sample (Figure 6a) it is possible to observe its heterogeneity, although such samples are in general considered as homogeneous. The analysis of the ϕ distribution

shows that the soil porosity is $(55\pm 5)\%$ (for 1880 points in the investigated plane). The large number of investigated points shows the ability of the GCT as a tool for detailed analysis of this physical property inside soil samples.

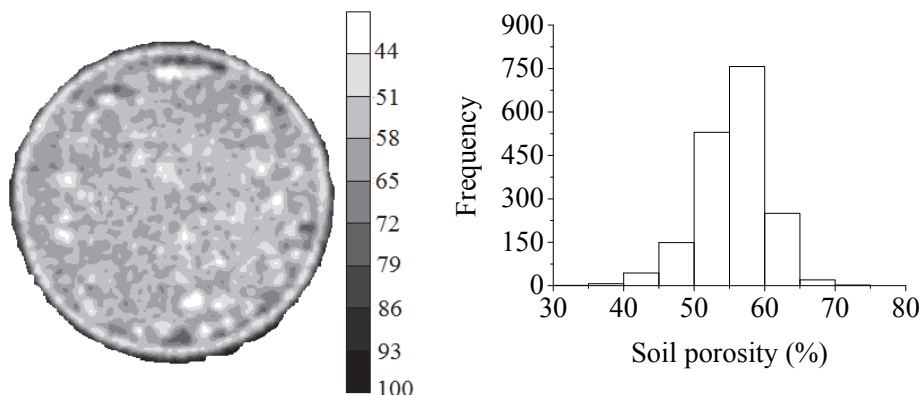


Fig. 6. (a) Tomographic image of an artificial soil sample packed inside a cylinder and (b) distribution of soil porosity (ϕ). The gray scale represents the distribution of ϕ , where white refers to the lowest ϕ value and black to the largest.

For the case of the soil clods presented earlier (Figure 4), the average values of ϕ ($n=18$) obtained by GCT and the traditional paraffin sealed methods were $36.2\pm 2.6\%$ and $36.6\pm 2.4\%$, respectively, showing a very good agreement between methods.

Having in mind the potential of tomography to give detailed analysis of soil bulk density and porosity the next two items explore the use of GCT in studies of soil porosity and structure changes due to natural and/or artificial processes.

4.2 Application of GCT to study soil crust

Soil surface sealing or crusting is an important phenomenon that may occur on soil surface as a result of clay migration/orientation processes and pore plugging. The impact of raindrops promotes the disintegration of soil aggregates and the dispersion of the clay particles in soil suspension. The finest particles in suspension migrate into soil pores along with water, plugging these pores. During the drying process, deposition, migration and orientation lead to the formation of a fine hard surface layer or soil crust (Baver et al., 1973). This layer produces soil surface flooding, increasing run-off volume, which can promote laminar and furrow erosions (Pagliai and Vignozzi, 1998; Pla, 1985).

In this sub-section the GCT was utilized to investigate soil surface crusting caused by application of sewage sludge as a fertilizer. The CT technique was employed as a tool to 1) identify differences in soil density due to the sewage sludge application and 2) determine the soil crust density and thickness in the compacted layers.

Soil samples for GCT analysis (Figure 7) come from an experimental field consisted of 3 treatments [2 sludge rates (SR) + 1 control (0SR)]. The sludge rates were calculated on the basis of dry weight of sludge, that correspond to: 10 and 80 t ha⁻¹ (1SR and 8SR). Soil samples were collected in steel rings of 3 and 5 cm (height and diameter) at the soil surface.

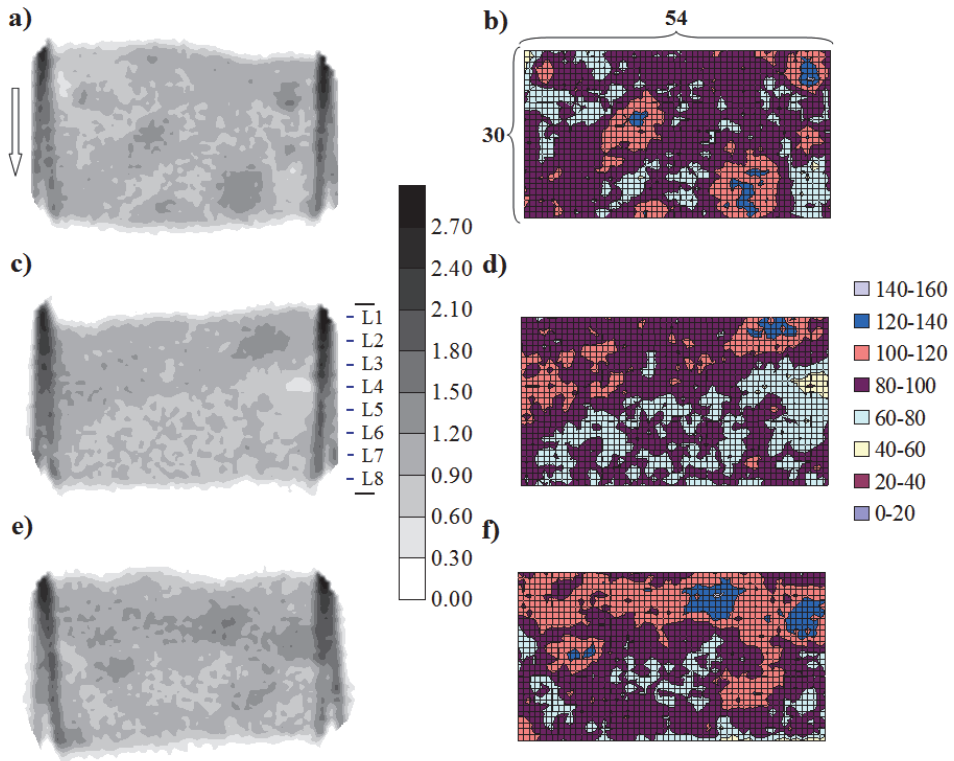


Fig. 7. (a) Absolute control sample (0SR), (b) Tomographic unit (TU) distribution (matrix of 54x30) map of the control sample; (c) Sample submitted to 10 t ha⁻¹ (1SR) of sewage sludge application; (d) TU distribution map of the sample 1SR; (e) Sample submitted to 80 t ha⁻¹ (8SR) of sewage sludge application and (f) TU distribution map of the sample 8SR. The gray scale represents the distribution of soil bulk density (ρ_s), where white refers to the lowest ρ_s value and black to the largest. The color scale represents the TU distribution for a matrix of data selected inside the soil image. The arrow indicates the direction of sampling at the soil surface and L represents soil layers of 3 mm each.

Soil images were obtained using a ¹³⁷Cs as radiation source due to the stainless steel rings. The tomographic images of soil samples were taken for vertical planes crossing the center of the sample.

GCT images (Figure 7) allowed a qualitative observation on the upper soil sample surface of the influence of the sewage sludge application. This result is more evident by the analysis of TU distribution maps (Figures 7b, d and f). For example, the comparison of the control sample (Figure 7b) and the sample with an application of 80 t ha⁻¹ of sewage sludge (Figure 7f) indicates a region with higher densities in the surface. This kind of crust was induced or incremented by the application of sewage sludge at the soil surface. Nonetheless, due to sampling variability, the sample submitted to the sewage application of 10 t ha⁻¹ did not present great changes in soil density at the surface in comparison to the control sample. This result is important as the appearance of a crust at the soil surface due to the sewage sludge

application as fertilizer, as already said, can affect water infiltration and favor laminar and furrow erosion.

To quantify the impact of sewage sludge application on soil bulk density, linear transects were constructed (Figure 8). Each transect presents the ρ_s distribution along soil depth.

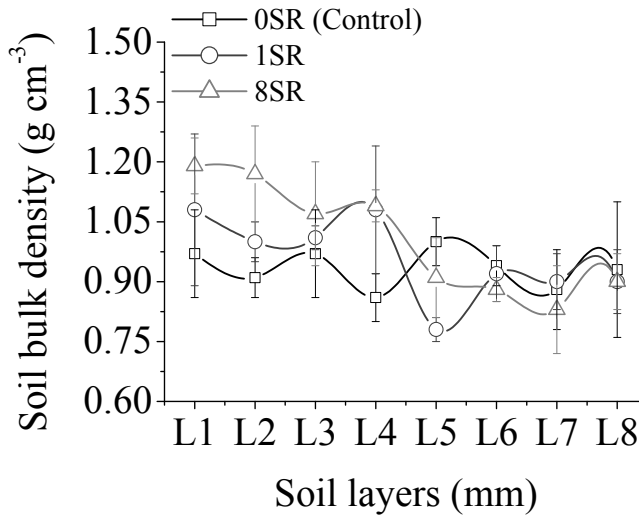


Fig. 8. Linear transects indicating soil bulk density (ρ_s) variation. Soil layers (L1 to L8) represent average values of three consecutive ρ_s determinations for layers of 1 mm. Error bars represent the standard deviation of the mean ($n=3$).

The analysis of the selected linear transects (Figure 8) show that the application of 80 t ha^{-1} of sewage sludge induces the appearance of a crust in the upper soil surface in comparison to the control samples. Also the samples submitted to 10 t ha^{-1} of this fertilizer present higher values of ρ_s at the soil surface. As expected, for the control samples (0SR) it is not possible to observe this more compacted region at the soil surface. For these samples the soil bulk density oscillates around a mean ($0.93 \pm 0.05 \text{ g cm}^{-3}$). This low average value of ρ_s is influenced by the amount of organic matter content in the samples collected at the soil surface.

After the layer L5 (13-15 mm) all soil samples practically present similar values of ρ_s ($0.92 \pm 0.03 \text{ g cm}^{-3}$ for 0SR, $0.91 \pm 0.01 \text{ g cm}^{-3}$ for 1SR, and $0.87 \pm 0.04 \text{ g cm}^{-3}$ for 8SR). This result shows the impact of sewage sludge application in the upper soil surface. However, it is important to mention that if another column of the soil matrix is selected for the analysis of ρ_s variation, distinct results of those presented can be obtained due to sample variability. On the other hand, when average values of ρ_s are evaluated considering all columns a similar behavior of that reported here would be obtained.

In order to avoid the influence of artifacts of the GCT images in the quantitative results the linear transects were selected about 3 mm below and above of the superior and inferior soil sample parts. To conclude the GCT analysis allowed determining that the thickness of the soil crust induced by the sewage sludge application varied from 2 to 4 mm.

4.3 Application of GCT to study soil structure changes

In this item two applications of the GCT technique to verify changes in soil structure will be presented. The first is related to the procedure of soil sampling and the second one to the application of wetting and drying cycles in samples used to evaluate soil water retention curves.

4.3.1 Soil sampling procedure effect on soil structure

Many soil scientists have investigated the influence of the sampling volume on the evaluation of soil physical properties such as, soil bulk density, air volume, water volume, and porosity (Rogasik et al., 1999). VandenBygaart and Protz (1999) tried to define a representative elementary area (REA) in the study of pedofeatures for quantitative analysis. They showed that there is a minimum area to represent pedofeatures and that it is not possible to make quantitative analyses for smaller areas. Baveye et al. (2002) showed the importance of the soil sampling volume in the determination of macroscopic parameters, and that small sampling volumes exhibit significant and seemingly erratic fluctuations.

Instruments used for soil sampling may also affect measurements. Camponez do Brasil (2000) showed that for four different soil sampling devices, certain soil physical properties could be strongly affected by the sampling process. The equipment could cause compaction of the samples, resulting in modifications of the porous system and consequently in soil structure.

Soil compaction and changes in soil structure can cause serious alterations of soil physical properties such as bulk density. Soil bulk density as said earlier is represented by the ratio between soil mass and soil volume. So, this property gives an idea of the percentage of voids that define soil structure. Low porosity represents a more compact region of the soil sample. These compacted regions can cause modifications in the soil water storage capacity and matric soil water potential, which are parameters used in irrigation and drainage management, and therefore have economic significance in agriculture.

Soil core samples were taken from a soil profile of a Geric Ferralsol according to FAO classification (FAO, 1998), from an experimental field located in Piracicaba, SP, Brazil (22°40'S; 47°38'W; 580 m above sea level). Two different soil sampling devices were used and correspond to inox cylinders of different sizes: (1) Sampler A (4.2 cm high, 2.7 cm i.d., 25 cm³ volume) and (2) Sampler B (5.3 cm high, 4.9 cm i.d., 100 cm³ volume).

All samplers permit the introduction of the steel cylinders in their inner space and soil samples are collected in these cylinders by a procedure that starts with a rubber mass falling from different heights to introduce the sampler containing the steel cylinder into the soil, down to the desired depth.

After complete introduction of the set into the soil, the surrounding soil is removed with a spade. The excavation is made carefully allowing the extraction of the cylinder containing the sample for density evaluation. Caution is needed during this process to minimize vibration, scissoring and compaction effects on the structure of the soil sample.

CT analysis was performed on 10 soil samples (5 from each soil sampler) carefully collected close to the soil surface. The pixel sizes were 1.0 x 1.0 mm for sampler A and 1.4 x 1.4 mm for sampler B. The pixel size was calculated by the ratio between the inner diameter of the soil sample and number of data of the reconstruction matrix (80x80). A ²⁴¹Am (59.54 keV) was used with an activity of 3.7 GBq.

For image analysis different concentric rectangular areas (from 0.4 to 6.7 cm² - sampler A and from 0.8 to 24.7 cm² - sampler B) were selected inside soil sample images (Figures 9 and

10), where the arithmetic means of TU were calculated and converted into ρ_s , giving a general idea of the spatial variability of this parameter, in depth as well as laterally, within the sample.

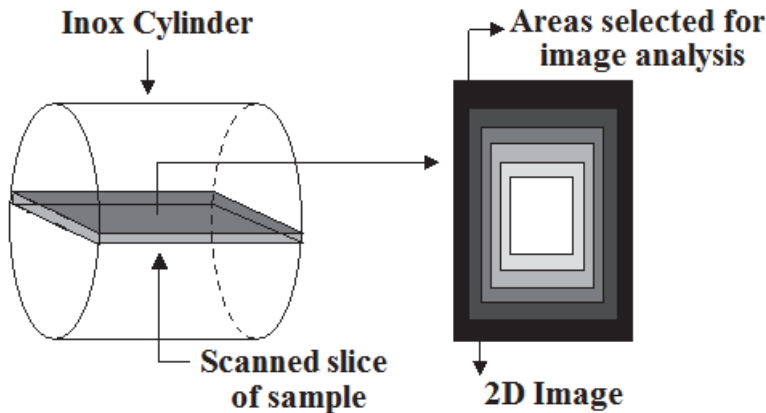


Fig. 9. Schematic diagram of the region selected for GCT image analysis and concentric rectangular areas utilized for soil sample quantitative analysis.

The mass attenuation coefficients for soil and water were 0.244 ± 0.003 and 0.199 ± 0.001 $\text{cm}^2 \text{g}^{-1}$, respectively. The obtained parameter calibration (α) used to calculate ρ_s (Equation 9) was 0.955 cm. The planes of image acquisition were vertical and the available data permitted a continuous 2-D analysis of the density distribution along the soil sample. The soil samples were air dried for several weeks before scanning.

Soil images (Figure 10) show a clear heterogeneity of ρ_s and the occurrence of larger values next to the edges of the samples. There is a density gradient for samples obtained by both soil sampler devices. However this ρ_s gradient seems to be more prominent for sampler A. For this sampler it is possible to observe a compaction at the bottom and at the top of the sample, due to the smaller internal diameter of the cylinder. Pires et al. (2004) have shown through of the analyses of transects of CT images that small soil-sampling volumes may induce compaction at the top and at the bottom of the soil sample.

The graph of ρ_s (Figure 11) confirms the existence of a density gradient from the center to the edge of samples. These results indicate that there is a compaction near the edge of sample and consequently a decrease in soil porosity. Decreases in soil porosity indicate variations in soil structure, which can affect soil hydraulic properties. Modifications in hydraulic properties can lead to important practical problems of water management of irrigated crops as said earlier.

In order to quantify the effect of sampler size in soil structure mathematical linear adjustments were constructed between ρ_s and A ($\rho_s = 0.09A + 1.16$, $r = 0.99$ for sampler A and $\rho_s = 0.02A + 0.84$, $r = 0.98$ for sampler B). Soil samples collected by sampler A presented the largest slope value, which indicates the great impact of this soil sampler device on sample structure in comparison to sampler B.

In order to avoid the effects of possible artifacts or fluctuations in images, as observed by other authors (Herman 1980; Paulus et al. 1999), in the evaluation of soil density, the quantitative analyses should be made selecting areas smaller than the real soil sample size

inside the cylinder. With this procedure we excluded the sample strip borders very close to the cylinder walls where the abrupt density changes (inox/soil) may cause the known image distortions.

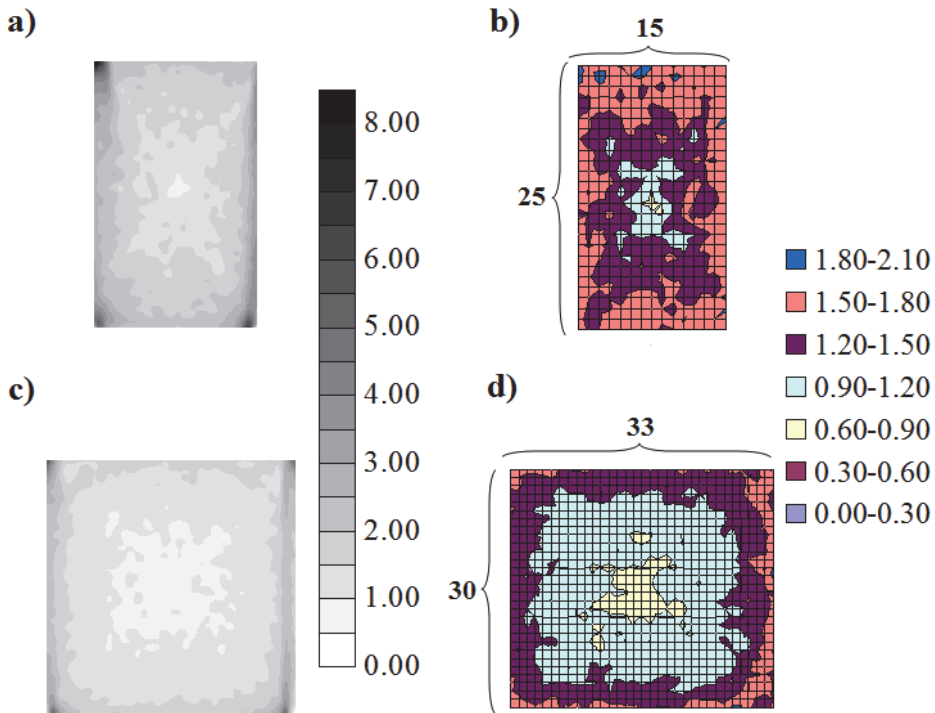


Fig. 10. (a) Soil image of the sample collected with the sampler A (4.2 cm high, 2.7 cm *i.d.*, 25 cm³ volume), (b) Tomographic unit (TU) distribution (matrix of 25x15) map of an area selected inside the sample presented in (a), (c) Soil image of the sample collected with the sampler B (5.3 cm high, 4.9 cm *i.d.*, 100 cm³ volume), (d) TU distribution (matrix of 30x33) map of an area selected inside the sample presented in (c). The gray scale represents the distribution of soil bulk density (ρ_s), where white refers to the lowest ρ_s value and black to the largest (in this specific case represent the attenuation by the inox cylinder wall). The color scale represents the ρ_s distribution for a matrix of data selected inside the soil image.

4.3.2 Soil structure changes due to wetting and drying cycles

Soil structure is influenced by several phenomena such as organic matter dynamics, soil genesis, human action, wetting/drying (W-D) cycles, and other (Kutílek and Nielsen, 1994). An important aspect of soil structure is the porosity, which consists of a continuous branching of pores of sizes classified in different categories like macro, meso and micropores (Oliveira et al., 1998). Adequate soil porosity is very important for soil aeration, water infiltration, and root distribution, allowing a better crop development. W-D cycles can cause great modifications of the structure of a soil, especially in pore distribution, which reflects the temporal and spatial distribution of soil water and, consequently, these processes can

affect soil water and nutrient retention and movement. These alterations have important practical consequences when calculating soil water storages and matric potentials, widely used in irrigation management.

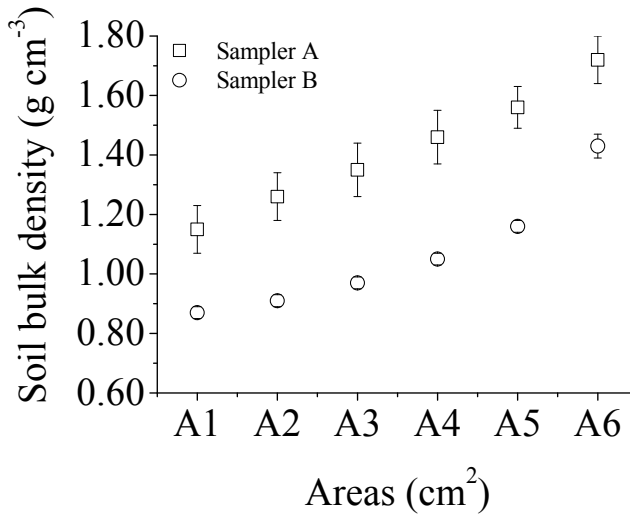


Fig. 11. Soil bulk density (ρ_s) variation with the cylinder diameter for the schematic areas (A) presented in figure 9 for the quantitative image analysis. Error bars represent the standard deviation of the mean ($n=5$).

The effect of W-D cycles on soil physical properties has been frequently cited in the literature (Sartori et al., 1985; Pagliai et al., 1987; Hussein and Adey, 1998; Rajaram and Erbach, 1999; Bresson and Moran, 2003; Pires et al., 2005). Soil structure, as a dynamic property, can be influenced by W-D cycles, pores being filled by water during wetting, with soil particles being rearranged irreversibly during drying. Thus, W-D cycles can affect soil resistance measured by cone penetration, particle cohesion, internal friction, aggregate size and their mechanical stability (Rajaram and Erbach, 1999). These cycles can also result in aggregate formation in non-aggregated soils restoring the damaged structure of some soils (Telfair et al., 1957; Newman and Thomasson, 1979).

According to Dexter (1988), W-D cycles affect directly soil aggregation due to the action of forces among soil particles and soil aggregates. Consequently, the soil porous system is strongly influenced by the sequences of wetting and drying cycles (Baumgartl, 1998). Wetting and drying processes produce small changes in the soil core sample volume, caused by stresses due to water/air interfaces originated from capillary forces. Therefore, after each new wetting step, the soil structure will undergo to a new state of energy, which most of the time promotes definitive changes in soil structure (Viana et al., 2004).

For this study a radioactive gamma-ray source of ^{241}Am was used. Circular lead collimators were adjusted and aligned between source and detector. Angular sample rotation steps $\Delta\phi$ were 2.25° until completing a scan of 180° , with linear steps Δr of 0.14 cm. The pixel size was 1.14×1.14 mm, calculated by the ratio between the inner diameter of the soil sample and number of pixels of the reconstruction matrix.

In order to avoid effects of possible artifacts or fluctuations in the images the quantitative analyses to determine the soil porosity was made selecting areas inside the cylinder smaller than the real soil sample size.

Core samples were taken from profiles of an Eutric Nitosol from an experimental field in Piracicaba, SP, Brazil. Six samples (3.0 cm high, 4.8 cm i.d., 55 cm³ volume) were collected at the soil surface (0 - 10 cm) with volumetric rings.

The chosen wetting process was the capillary rise, which is used during soil water retention determinations. The procedure of wetting consisted initially in maintaining a level of water 0.3 cm from the bottom of the cylinder during 2 hours and after this the water level was elevated to just below the top of the cylinder. Forty eight hours were necessary to obtain complete saturation of soil samples by capillary rise in order to avoid entrapped air bubbles, which can cause slaking of soil aggregates, changing soil structure.

The procedure used to dry samples was the application of 4.0 MPa of pressure (P) on the saturated soil sample, driving away soil water retained at pressures below P (Klute, 1986), inside a Richards apparatus. Soil samples were submitted to none (T0WD) and nine (T9WD) W-D cycles. GCT images were obtained at fixed water contents, to avoid differences in soil images due to differences in the residual water content after each treatment.

The procedure used to obtain fixed water contents, after W-D cycles, was to maintain samples in contact with air until a residual value of θ . When samples, after T0WD and T9WD, reached this residual water content they were involved in plastic film, to minimize water loss, and submitted to CT scanning.

Mass attenuation coefficients were obtained using the method described in Ferraz and Mansell (1979) and the following results were obtained: 0.328 ± 0.003 (soil) and 0.199 ± 0.001 cm² g⁻¹ (water). The calibration of GCT presented a high positive correlation coefficient ($r=0.99$). Qualitative analyses of changes in soil structure were obtained by soil image analysis (Figure 12).

From the GCT images (Figure 12) it was possible to visualize modifications in soil structure. In the T0WD sample (Figures 12a and 12b), the existence of compacted regions can be seen at the upper and at the lower layers (Layers A and F) of the sample. Higher ρ_s at layer A was a characteristic of the investigated sample while that at the bottom probably was due to sampling preparation that, in this case consisted in making the sample bottom flat with a sharp blade. However, after the application of nine W-D cycles (Figures 12c and 12d) to the same sample it is possible to observe that ρ_s values in the investigated layers decreased, with more evidence in the more compacted layers.

These results indicate that significant modifications in soil water retention characteristics can occur due to W-D cycles. The changes of the soil pore systems will affect water retention properties due to changes in ϕ . This result can represent a repair of soil structure, having as an impact increases in the water storing capacity, important for plant and root development.

A better analysis of changes in soil structure with the W-D cycles along depth can be obtained through quantitative analysis of ϕ variation (Figure 13). To investigate the effects of W-D cycles on ϕ , each investigated sample was divided in six regions, named from A to F as schematically presented in figure 12. In this particular experimental setting up, each subsequent layer was around 4.5mm apart one from the other.

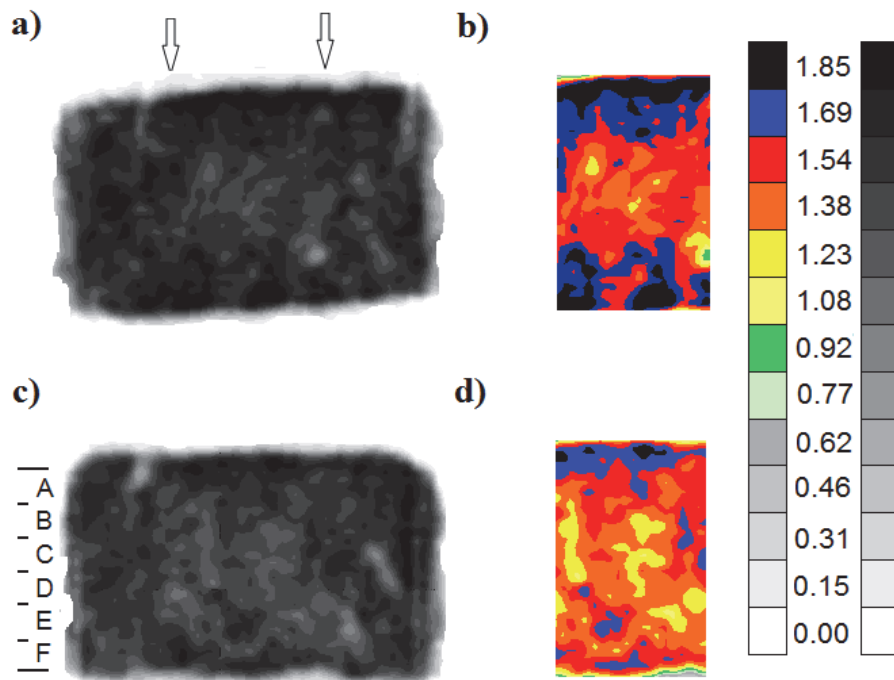
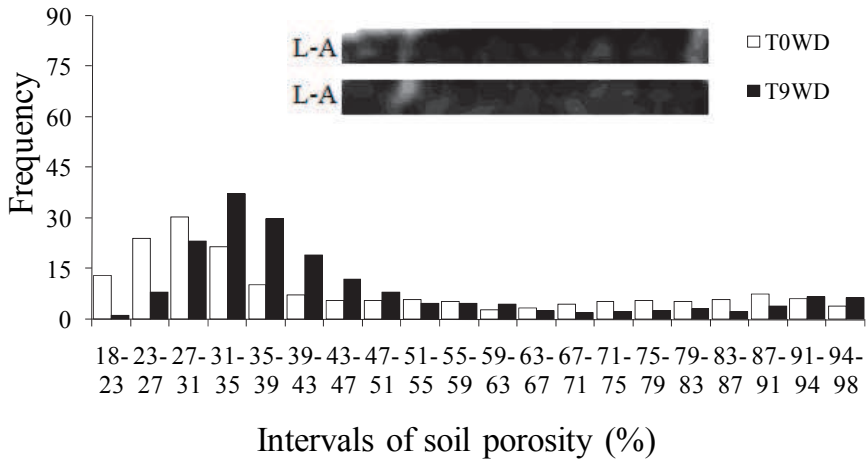


Fig. 12. (a) 2-D tomographic images of core samples used to evaluate soil bulk density (ρ_s) and porosity by image (ϕ) variations of samples not submitted to wetting and drying (W-D) cycles, (b) Tomographic unit (TU) distribution (matrix of 80×20) map of an area selected inside the sample presented in (a), (c) Soil image of the sample submitted to 9 W-D cycles by the capillary rise method, (d) TU distribution map of an area selected inside the sample presented in (c). The gray and color scales represent the distribution of ρ_s . For the gray scale white refers to the lowest ρ_s value and black to the largest. Arrows indicate the region (matrix of 1600 (80×20) TU values) of soil structure change analysis (b-d). Letters A to F represent soil layers defined for quantitative analysis.

As it can be seen, the application of W-D cycles caused increases in ϕ mainly for the layers (L-A and L-F) near to the border of samples (Figures 13a and 13f). This result is characterized by the increase in the frequency of higher ϕ values. The application of W-D cycles expands the ϕ distribution. This result means that the W-D cycles can induce the appearance of large macropores in the soil samples and a more heterogeneous distribution of ϕ . This result is particularly interesting to soil science because it represents an improvement of soil structure.

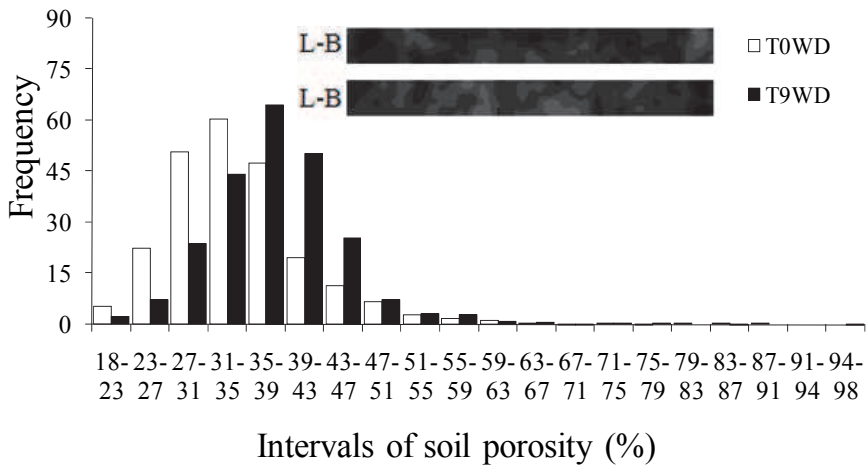
The analyses of results along depth show that the changes in ϕ for intermediate depths (L-C and L-D) are smoother (Figures 13c and 13d) than those for layers next to the sample border. This result can be explained by the soil sampling procedure and by the fact that the most significant changes in ϕ occur in the most compacted regions in figure 12 (layers A, E and F). It is expected that the most significant changes occur in the outer layers, because the soil in these regions can also freely expand with the W-D cycles.

Layer A (L-A)

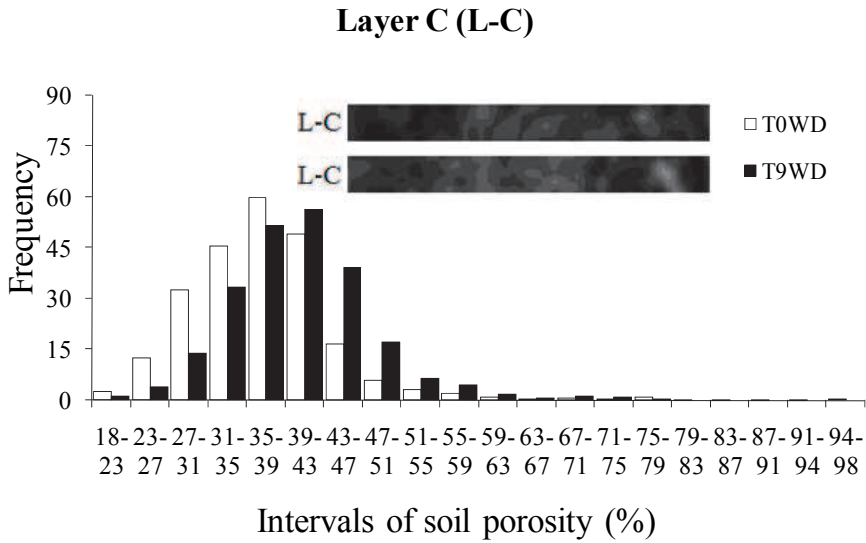


(a)

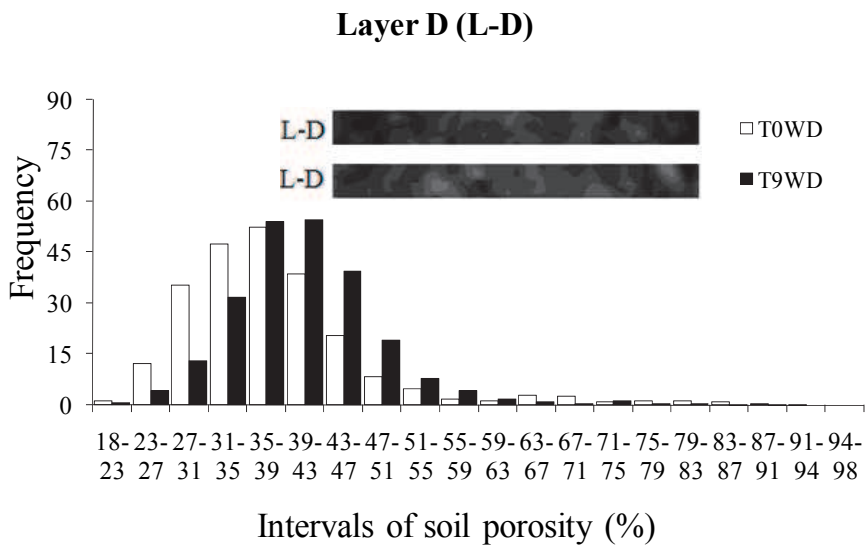
Layer B (L-B)



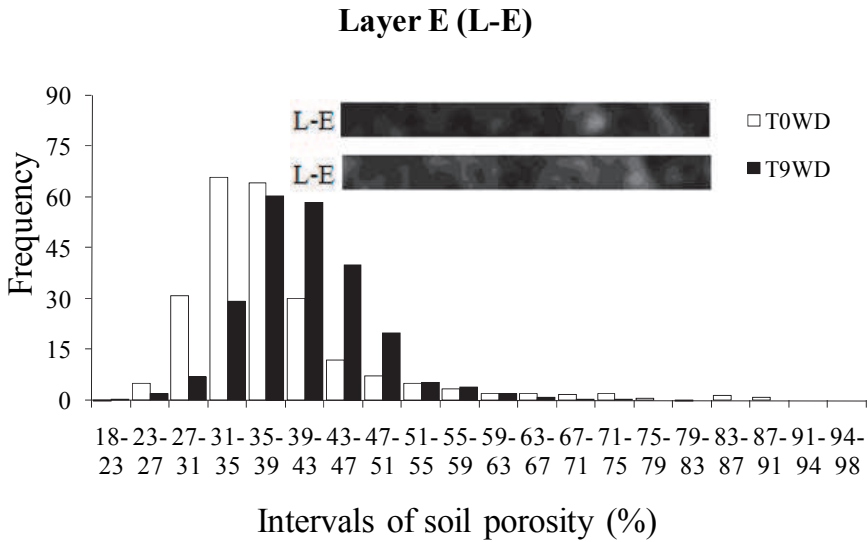
(b)



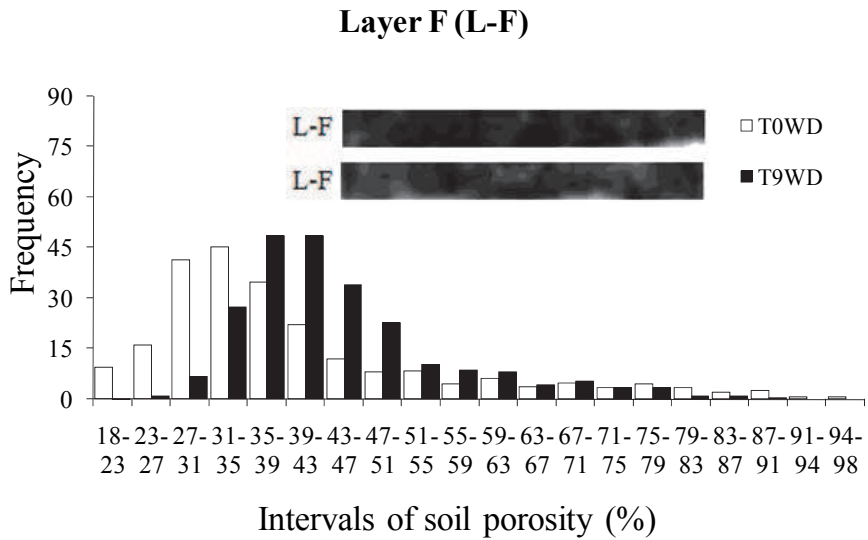
(c)



(d)



(e)



(f)

Fig. 13. (a-f) Changes in soil porosity (ϕ) along soil sample depth. T0WD and T9WD represents soil samples not submitted to wetting and drying (W-D) cycles and submitted to 9 W-D, respectively. Values of ϕ represent average of six replicates. The layer pictures (L slices) presented on the graphs is only illustrative for the specific sample presented in figures 12a and 12c.

5. Future expectations on the use of CT in soil physics

From the discussion on the GCT technique it can clearly be seen that it has been applied with success in the analysis of physical properties of soils. With the investments that have been made in equipment exclusively projected for this purpose it is expected that CT will gradually be able to yield more representative results of these properties.

New tomographic models based on the use of radiation from synchrotron light, positrons and neutrons may become interesting alternatives for the study of soil physical characteristics, opening the possibility of obtaining images of better resolution and also presenting greater sensitivity to monitor soil water content changes. The development of new microtomographs of 3rd and 4th generation for specific use in soil science can also be an interesting alternative for dynamic soil water studies.

Studies of the dynamics of root growth can also be carried out in a non invasive way using microtomographs. Systems that make use of X-ray or synchrotron light beams can be used with success in this type of investigation since they allow the analysis of samples of very large size such as 20 cm or more. Third generation scanners of X-rays and with micrometric resolution allow quick analyses of soil structure in 3D, which may be useful for dynamic processes that occur inside the soil.

The broadening of the use of the 3rd generation X-ray microtomography that work in soil science would certainly lead to new applications of CT that would bring new developments related to soil structure, like more realistic studies on tortuosity, connectivity, shape, size, and pore distribution. Such information, until now not well explored will help in a significant way the construction of models for flow processes involving hydraulic conductivity, solute infiltration, root development, and would produce more representative images for the numeric simulation of these important physical processes that take place in soils.

6. Acknowledgment

The authors would like to thank the Brazilian agency 'Conselho Nacional de Desenvolvimento Científico e Tecnológico' (CNPq) for the research fellowships to Klaus Reichardt, Luiz F. Pires and Osny O.S. Bacchi.

7. References

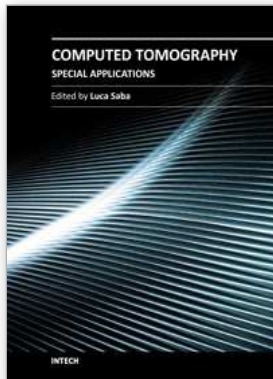
- Appoloni, C.R., Macedo, A., Fernandes, C.P. & Philippi, P.C. (2002). Characterization of porous microstructure by X-ray microtomography. *X-Ray Spectrometry*, 31, 124-127
- Balogun, F.A. & Cruvinel, P.E. (2003). Compton scattering tomography in soil compaction study. *Nuclear Instruments and Methods in Physics Research A*, 505, 502-507
- Baumgartl, Th. (1998). Physical soil properties in specific fields of application especially in anthropogenic soils. *Soil and Tillage Research*, 47, 51-59
- Baver, L.D., Gardner, W.J. & Gardner, W.R. (1973). *Física de suelos*, Union Tipográfica Editorial Hispano Americana, Mexico
- Baveye, P., Rogasik, H., Wendroth, O., Onasch, I. & Crawford, J.W. (2002). Effect of sampling volume on the measurement of soil physical properties: simulation with X-ray tomography data. *Measurement Science Technology*, 13, 775-784
- Biassusi, M., Pauletto, E.A. & Crestana, S. (1999). Estudo da deformação de um vertissolo por meio da tomografia computadorizada de dupla energia simultânea. *Revista Brasileira de Ciência do Solo*, 23, 1-7

- Brandsma, R.T., Fullen, M.A., Hocking, T.J. & Allen, J.R. (1999). An X-ray scanning technique to determine soil macroporosity by chemical mapping. *Soil and Tillage Research*, 50, 95-98
- Braz, D., Barroso, R.C., Lopes, R.T., Anjos, M.J. & Jesus, E.F.O. (2001). Evaluation of scatter-to-primary ratio in soil CT-imaging. *Radiation Physics and Chemistry*, 61, 747-751
- Bresson, L.M. & Moran, C.J. (2003). Role of compaction versus aggregate disruption on slumping and shrinking of repacked hardsetting seedbeds. *Soil Science*, 168, 585-594
- Brooks, R.A., Mitchell, L.G., O'Conner, C.M. & Di Chiro, G. (1981). On the relationship between computed tomography numbers and specific gravity. *Physics in Medicine and Biology*, 26, 141-147
- Camponez do Brasil, R.P. (2000). Influência das técnicas de coleta de amostras na determinação das propriedades físicas do solo. Master Thesis, Universidade de São Paulo, Piracicaba, Brazil, 110p
- Cesareo, R. & Giannini, M. (1980). Elemental analysis by means of X-ray attenuation measurements. *Nuclear Instruments and Methods*, 169, 551-555
- Cesareo, R., Assis, J.T. & Crestana, S. (1994). Attenuation coefficients and tomographic measurements for soil in the energy range 10-300 keV. *Applied Radiation and Isotopes*, 45, 613-620
- Chase, G.D. & Rabinowitz, J.L. (1968). *Principles of radioisotope methodology*, Burgess Publishing Co., Minneapolis, USA
- Coles, M.E., Hazlett, R.D., Muegge, E.L., Jones, K.W., Andrews, B., Dowd, B., Siddons, P., Peskin, A., Spanne, P. & Soll, W. (1998). Developments in synchrotron X-ray microtomography with applications to flow in porous media. *SPE Reservoir Evaluation and Engineering*, 1, 288-296
- Colgate, S.A. (1952). Gamma-ray absorption measurements. *Physics Review*, 87, 592-600.
- Cormack, A.M. (1963). Representation of a foundation by its line with some radiological application. *Journal of Applied Physics*, 34, 2722-2727
- Costa, J.C. (2011). Tamanho do colimador e espessura da amostra em medidas do coeficiente de atenuação de raios gama do solo. Master Thesis, Universidade Estadual de Ponta Grossa, Ponta Grossa, Brazil, 105p
- Crestana, S., Mascarenhas, S. & Pozzi-Mucelli, R.S. (1985). Static and dynamic 3D studies of water in soil using computed tomographic scanning. *Soil Science*, 140, 326-332
- Crestana, S., Cesareo, R. & Mascarenhas, S. (1986). Using a computed tomography miniscanner in soil science. *Soil Science*, 142, 56-61
- Crestana, S., Cruvinel, P.E., Vaz, C.M.P., Cesareo, R., Mascarenhas, S. & Reichardt, K. (1992). Calibração e uso de um tomógrafo computadorizado em ciência do solo. *Revista Brasileira de Ciência do Solo*, 16, 161-167
- Cruvinel, P.E., Cesareo, R., Crestana, S. & Mascarenhas, S. (1990). X- and gamma-rays computerized minitomograph scanner for soil science. *IEEE Transactions on Instrumentation and Measurement*, 39, 745-750
- Dexter, A.R. (1988). Advances in characterization of soil structure. *Soil and Tillage Research*, 11, 199-238
- Elliot, T.R. & Heck, R.J. (2007). A comparison of optical and X-ray CT technique for void analysis in soil thin section. *Geoderma*, 141, 60-70
- Elzeftawy, A., Mansell, R.S. & Selim, H.M. (1976). Distribution of water and herbicide in Lakeland sand during initial stages of infiltration. *Soil Science*, 122, 297-307
- Fante Júnior, L., Oliveira J.C.M., Bassoi, L.H., Vaz, C.M.P., Macedo, A., Bacchi, O.O.S., Reichardt, K., Cavalcanti, A.C. & Silva, F.H.B.B. (2002). Tomografia

- Computadorizada na avaliação da densidade de um solo do semi-árido brasileiro. *Revista Brasileira de Ciência do Solo*, 26, 835-842
- FAO. (1998). *World reference base for soil resources*, FAO, ISRIC and ISSS, Rome, Italy
- Ferraz, E.S.B. (1974). Determinação simultânea de densidade e umidade de solos por atenuação de raios gama do ^{137}Cs e ^{241}Am . Free Teaching Thesis, Universidade de São Paulo, Piracicaba, Brazil, 120p
- Ferraz, E.S.B. & Mansell, R.S. (1979). Determining water content and bulk density of soil by gamma-ray attenuation methods. *Technical Bulletin*, 807, IFAS, Flórida, USA 51p
- Flint, A.L. & Flint, L.E. (2002). The solid phase: Particle density. In: Dane, J.H. & Topp, G.C. (Eds.), *Methods of soil analysis. Part 4. Physical Methods*. ASA, SSSA, Madison, USA p.229-240
- Gantzer, C.J. & Anderson, S.H. (2002). Computed tomographic measurement of macroporosity in chisel-disk and no-tillage seedbeds. *Soil and Tillage Research*, 64, 101-111
- Hainsworth, J.M. & Aylmore, L.A.G. (1983). The use of computer-assisted tomography to determine spatial distribution of soil water content. *Australian Journal of Soil Research*, 21, 435-443
- Herman, G.T. (1980). *Image reconstruction from projections*, Academic Press, London, UK
- Horgan, G.W. (1998). Mathematical morphology for analyzing soil structure from images. *European Journal of Soil Science*, 49, 161-173
- Hounsfield, G.N. (1973). Computerized transverse axial scanning (tomography). 1. Description of system. *British Journal of Radiology*, 46, 1016-1022
- Hussein, J. & Adey, M.A. (1998). Changes in microstructure, voids and b-fabric of surface samples of a Vertisol caused by wet/dry cycles. *Geoderma*, 85, 63-82
- Jégou, D., Brunotte, J., Rogasik, H., Capowicz, Y., Diestel, H., Schrader, S. & Cluzeau, D. (2002). Impact of soil compaction on earthworm burrow systems using X-ray computed tomography: preliminary study. *Soil Biology*, 38, 329-336
- Jenkins, R., Gould, R.W. & Gedcke, D. (1981). *Qualitative X-ray spectrometry*, Marcel Dekker, New York, USA
- Kak, A.C. & Slaney, M. (1988). *Principles of computerized tomographic imaging*, IEEE Press, New York, USA
- Kaplan, I. (1963). *Nuclear Physics*, Addison-Wesley Publishing Co., Reading, USA
- Klute, A. (1986). Water retention: laboratory methods. In: Black, C.A. (Ed.), *Methods of soil analysis. I. Physical and mineralogical methods*. ASA, SSSA, Madison, USA, p.635-662
- Kutílek, M. & Nielsen, D.R. (1994). *Soil hydrology*, Catena Verlag, Berlin, Germany
- Langmaak, M., Schrader, S., Rapp-Bernhardt, U. & Kotze, K. (2002). Soil structure rehabilitation of arable soil degraded by compaction. *Geoderma*, 105, 141-152
- Li, D., Velde, B. & Zhang, T. (2004). Observations of pores and aggregates during aggregation in some clay-rich agricultural soils as seen in 2D image analysis. *Geoderma*, 118, 191-207
- Lopes, R.T., Bessa, A.P., Braz, D. & Jesus E.F.O. (1999). Neutron computerized tomography in compacted soil. *Applied Radiation and Isotopes*, 50, 451- 458
- Martz, H.E., Azevedo, S.G., Brase, J.M., Waltjen, K.E. & Schnerberk, D.J. (1990). Computed tomography systems and their industrial applications. *Applied Radiation and Isotopes*, 41, 943-961
- MICROVIS. (2000). *Programa de reconstrução e visualização de imagens tomográficas*, Embrapa Instrumentação Agropecuária, São Carlos, Brazil

- Modolo, A.J., Fernandes, H.C., Naime, J.M., Schaefer, C.E.G.R., Santos, N.T. & Silveira, J.C.M. (2008). Avaliação do ambiente solo-semente por meio da tomografia computadorizada. *Revista Brasileira de Ciência do Solo*, 32, 525-532
- Naime, J. de M. (1994). Projeto e construção de um minitomógrafo portátil para estudo de ciência do solo e plantas em campo. Master Thesis, Universidade de São Paulo, São Carlos, Brazil, 87p
- Naime, J. de M. (2001). Um novo método para estudos dinâmicos, in situ, da infiltração da água na região não-saturada do solo. Ph.D. Thesis, Universidade de São Paulo, São Carlos, Brazil, 145p
- Newman, A.C.D. & Thomasson, A.J. (1979). Rothamsted studies of soil structure: III. Pore size distributions and shrinkage processes. *Journal of Soil Science*, 30, 415-439
- Oliveira, J.C.M., Appoloni, C.R., Coimbra, M.M., Reichardt, K., Bacchi, O.O.S., Ferraz, E., Silva, S.C. & Galvão Filho, W. (1998). Soil structure evaluated by gamma-ray attenuation. *Soil and Tillage Research*, 48, 127-133
- Pagliai, M., La Marca, M. & Lucamante, G. (1987). Changes in soil porosity in remolded soils treated with poultry manure. *Soil Science*, 144, 128-140
- Pagliai, M. & Vignozzi, N. (1998). Use of manure for soil improvement. In: Wallace, A. & Terry, R.E. (Eds.), *Handbook of soil conditions: Substances that enhance the physical properties of soil*. Marcel Dekker, New York, USA
- Paulus, M.J., Sari-Sarraf, H., Gleason, S.S., Bobrek, M., Hicks, J.S., Johnson, D.K., Behel, J.K., Thompson, L.H. & Allen, W.C. (1999). A new X-ray computed tomography system for laboratory mouse imaging. *IEEE Transactions on Nuclear Science*, 46, 558-564
- Pedrotti, A., Pauleto E.A., Crestana S., Cruvinel P.E., Vaz, C.M.P., Naime, J.M. & Silva, A.M. (2003). Planosol soil sample size for computerized tomography measurement of physical parameters. *Scientia Agricola*, 60, 735-740
- Perret, J., Prasher, S.O., Kantzas, A. & Langford, C. (1999). Three-dimensional quantification of macropore networks in undisturbed soil cores. *Soil Science Society of America Journal*, 63, 1530-1543
- Petrovic, A.M., Siebert, J.E. & Rieke, P.E. (1982). Soil bulk density analysis in three dimensions by computed tomographic scanning. *Soil Science Society of America Journal*, 46, 445- 450
- Phogat, V.K., Aylmore, L.A.G. & Schuller, R.D. (1991). Simultaneous measurement of the spatial-distribution of soil-water content and bulk-density. *Soil Science Society of America Journal*, 55, 908-915
- Pires, L.F., Bacchi, O.O.S. & Reichardt, K. (2004). Damage to soil physical properties caused by soil sampler devices assessed by gamma ray computed tomography. *Australian Journal of Soil Research*, 42, 857-863
- Pires, L.F., Bacchi, O.O.S. & Reichardt, K. (2005). Gamma ray computed tomography to evaluate wetting/drying soil structure changes. *Nuclear Instruments and Methods in Physics Research B*, 229, 443-456
- Pires, L.F., Arthur, R.C.J., Bacchi, O.O.S. & Reichardt, K. (2007). Application of gamma-ray computed tomography to evaluate the radius of influence of soil solution extractors and tensiometers. *Nuclear Instruments and Methods in Physics Research B*, 259, 969-974
- Pires, L.F., Cooper, M., Cássaro, F.A.M., Bacchi, O.O.S., Reichardt, K. & Dias, N.M.P. (2008). Micromorphological analysis to characterize structure modifications of soil samples submitted to wetting and drying cycles. *Catena*, 72, 297-304
- Pires, L.F., Borges, J.A.R., Bacchi, O.O.S. & Reichardt, K. (2010). Twenty-five years of computed tomography in soil physics: A literature review of the Brazilian contribution. *Soil and Tillage Research*, 110, 197-210

- Pires, L.F., Cássaro, F.A.M., Bacchi, O.O.S. & Reichardt, K. (2011a). Non-destructive image analysis of soil surface porosity and bulk density dynamics. *Radiation Physics and Chemistry*, 80, 561-566
- Pires, L.F., Arthur, R.C.J., Bacchi, O.O.S. & Reichardt, K. (2011b). Representative gamma-ray computed tomography calibration for applications in soil physics. *Brazilian Journal of Physics*, 41, 21-28
- Pires, L.F., Cássaro, F.A.M., Saab, S.C. & Brinatti, A.M. (2011c). Characterization of changes in soil porous system by gamma-ray tomography. *Nuclear Instruments and Methods in Physics Research A*, 644, 68-71
- Pla, I. (1985). A routine laboratory index to predict the effects of soil sealing on soil and water conservation. In: *International Symposium on the assessment of soil surface sealing and crusting*. Ghent, Belgium. ISSS. AISS. IBG, pp.154-162
- Rajaram, G. & Erbach, D.C. (1999). Effect of wetting and drying on soil physical properties. *Journal of Terramechanics*, 36, 39-49
- Rasiah, V. & Aylmore, L.A.G. (1998). Computed tomography data on soil structural and hydraulic parameters assessed for spatial continuity by semivariance geostatistics. *Australian Journal of Soil Research*, 36, 485-493
- Rogasik, H., Crawford, J.W., Wendroth, O., Young, I.M., Joshko, M. & Ritz, K. (1999). Discrimination of soil phases by dual energy X-ray tomography. *Soil Science Society of America Journal*, 63, 741-751
- Sartori, G., Ferrari, G.A. & Pagliari, M. (1985). Changes in soil porosity and surface shrinkage in a remolded, saline clay soil treated with compost. *Soil Science*, 139, 523-530
- Stenstrom, M., Olander, B., Carlsson, C.A., Alm Carlsson, G., Lehto-Axtelius, D. & Hakanson, R. (1998). The use of computed microtomography to monitor morphological changes in small animals. *Applied Radiation and Isotopes*, 49, 565-570
- Taina, I.A., Heck, R.J. & Elliot, T.R. (2008). Application of X-ray computed tomography to soil science: A literature review. *Canadian Journal of Soil Science*, 88, 1-20
- Telfair, D., Gardner, M.R. & Miars, D. (1957). The restoration of a structurally degenerated soil. *Soil Science Society of America Journal*, 21, 131-134
- Vandenbygaart, A.J. & Protz, R. (1999). The representative elementary area (REA) in studies of quantitative soil micromorphology. *Geoderma*, 89, 333-346
- Viana, J.H.M., Fernandes Filho, E.I. & Schaefer, C.E.G.R. (2004). Efeitos de ciclos de umedecimento e secagem na reorganização da estrutura microgranular de latossolos. *Revista Brasileira de Ciência do Solo*, 28, 11-19
- Vontobel, P., Lehmann, E.H., Hassanein, R. & Frei, G. (2006). Neutron tomography: Method and applications. *Physica B*, 385/386, 475-480
- Voronov, R.S., VanGordon, S.B., Sikavitsas, V.I. & Papavassiliou, D.V. (2010). Distribution of flow-induced stresses in highly porous media. *Applied Physics Letters*, 97, 24101-24103
- Vaz, C.M.P., Crestana, S., Mascarenhas, S., Cruvinel, P.E., Reichardt, K. & Stolf, R. (1989). Using a computed tomography miniscanner for studying tillage induced soil compaction. *Soil Technology*, 2, 313-321
- Wang, C.H., Willis, D.L. & Loveland, W.D. (1975). Characteristics of ionizing radiation, In: Wang, C.H., Willis, D.L. & Loveland, W.D. (Eds.), *Radiotracer methodology in the biological, environmental, and physics sciences*. Prentice-Hall, Englewood Cliffs, p.39-74
- Wildenschild, D., Hopmans, J.W., Vaz, C.M.P., Rivers, M.L., Rikard, D. & Christensen, B.S.B. (2002). Using X-ray computed tomography in hydrology: systems, resolutions, and limitations. *Journal of Hydrology*, 267, 285-297
- Wingler, B., Kahle, A. & Hennion, B. (2006). Neutron radiography of rocks and melts. *Physica B*, 385/386, 933-934



Computed Tomography - Special Applications

Edited by Dr. Luca Saba

ISBN 978-953-307-723-9

Hard cover, 318 pages

Publisher InTech

Published online 21, November, 2011

Published in print edition November, 2011

CT has evolved into an indispensable imaging method in clinical routine. The first generation of CT scanners developed in the 1970s and numerous innovations have improved the utility and application field of the CT, such as the introduction of helical systems that allowed the development of the "volumetric CT" concept. Recently interesting technical, anthropomorphic, forensic and archeological as well as paleontological applications of computed tomography have been developed. These applications further strengthen the method as a generic diagnostic tool for non destructive material testing and three dimensional visualization beyond its medical use.

How to reference

In order to correctly reference this scholarly work, feel free to copy and paste the following:

Luiz Fernando Pires, Fábio Augusto Meira Cássaro, Osny Oliveira Santos Bacchi and Klaus Reichardt (2011). Gamma-Ray Computed Tomography in Soil Science: Some Applications, *Computed Tomography - Special Applications*, Dr. Luca Saba (Ed.), ISBN: 978-953-307-723-9, InTech, Available from: <http://www.intechopen.com/books/computed-tomography-special-applications/gamma-ray-computed-tomography-in-soil-science-some-applications>

INTECH
open science | open minds

InTech Europe

University Campus STeP Ri
Slavka Krautzeka 83/A
51000 Rijeka, Croatia
Phone: +385 (51) 770 447
Fax: +385 (51) 686 166
www.intechopen.com

InTech China

Unit 405, Office Block, Hotel Equatorial Shanghai
No.65, Yan An Road (West), Shanghai, 200040, China
中国上海市延安西路65号上海国际贵都大饭店办公楼405单元
Phone: +86-21-62489820
Fax: +86-21-62489821

© 2011 The Author(s). Licensee IntechOpen. This is an open access article distributed under the terms of the [Creative Commons Attribution 3.0 License](#), which permits unrestricted use, distribution, and reproduction in any medium, provided the original work is properly cited.